Supporting Information

Klauss et al. 10.1073/pnas.1206266109

SI Text

SI Materials and Methods. ***Experimental details. Photosystem II (PSII) sample preparation.*** PSII membrane particles with high O_2-evolution activity (approximately 1,100 μmol O_2 per mg chlorophyll and h, at 28 °C) were prepared from spinach as described elsewhere (1, 2) and stored at −80 °C. For photothermal beam deflection (PBD) experiments, the preparations were thawed and washed in buffer A (1 M glycine betaine, 15 mM NaCl, 5 mM $MgCl_2$, 5 mM $CaCl_2$, 15 mM MES, pH 6.2). The pellet of PSII membranes was resuspended at 80 μg/mL of chlorophyll in buffer A, and 20 μM of 2,6-dichloro-*p*-benzoquinone (DCBQ) were added as artificial electron acceptor. For experiments in D_2O, buffer A was prepared with D_2O (99% purity) and a pD of 6.2 was adjusted (pH meter reading of 5.8).

PBD experiments were carried out using the previously described setup (3, 4). For a scheme of the experimental protocol, see Fig. S1*A*. About 100 mL of PSII suspension were kept in a dark reservoir on ice (under gentle stirring) and pumped first for thermostatization through a laboratory-built heat exchanger, and then into the thermostated flow-through cuvette (3-mm optical path). The temperature of the sample was determined in the cuvette and close to the position of the measuring light beam. A Q-switched, frequency-doubled Nd:YAG laser (Continuum Minilight; 532 nm, pulse duration 5 ns) served as the excitation light source (pump flash). The laser pulse energy was determined for each flash by an energy meter (Sensor und Lasertechnik) and was 5 ± 0.5 μJ in standard experiments, irradiating a sample area of about 5 mm^2. Each signal was normalized to the excitation pulse energy prior to averaging. In the H_2O/D_2O exchange experiments the pump laser energy was approximately 9 μJ. An infrared continuous-wave laser diode (920 nm) served as the measuring light source (probe beam). The probe beam was focused on a two-element photodiode serving as a detector of the PBD signals. A second pulsed Nd:YAG laser (Continuum Inlight; 532 nm, pulse duration 5 ns, attenuated to approximately 10 mJ cm^{-2}), impinging perpendicular to the probe beam onto the sample, was used as an actinic light source for stepping of PSII through the S-state cycle (700-ms spacing of flashes). Data acquisition was done on a PC system using in-house software. The electrical bandwidth of the detector system was 100 KHz. The sampling frequency was 1 MHz and the number of data points was reduced by appropriate averaging of 10 data points. This protocol results in data points of the PBD signal that are spaced by 10 μs and are essentially unaffected by the bandwidth of the detection system. The experiment (temperature control, sample exchange, laser flashes, laser energy control, data acquisition) was synchronized by appropriate trigger electronics.

PBD analysis. The PBD signal amplitude (X) is proportional to the change in refractive index in the sample during the photochemistry, which involves two major contributions (5): (*i*) The thermal part is caused by heat release (ΔQ) after flash excitation and the resulting decrease of the specific density. (*ii*) The nonthermal part (ΔN) is caused by changes in the density of the sample owing to structural changes that increase (expansion) or decrease (contraction) the effective protein volume. Both parts can be separated by temperature variation (3–6). Then, from ΔN, an apparent volume change (ΔV) in the sample can be estimated as detailed elsewhere (3, 7):

$$\Delta V \approx \frac{\Delta N}{\phi_0\ \phi_{\mathrm{sat}} X_{\mathrm{reference}}} 25\ \text{Å}^3, \qquad \textbf{[S1]}$$

where $X_{\mathrm{reference}}$ is the PBD signal (at 20 °C) of a calorimetric reference [i.e., a dye such as bromocresol purple (BCP, see Fig. S7) or PSII centers with permanently reduced primary quinone acceptor, Q_A^- ("closed centers"; see Fig. S3), in which 100% of the absorbed photon energy is thermalized rapidly].

The value of Φ_0, the quantum yield of the light-driven reactions, could be estimated only roughly. At 532 nm, loss processes resulting from excitation of uncoupled carotenoids and quenching of excited states by the artificial electron acceptor decreased the value of Φ_0 from its maximal value. We estimated that Φ_0 was in the range from 60–80%. Moreover, the used excitation energy was in a range in which partial saturation of the photochemistry occurred (3), resulting in a value for Φ_{sat} of 70% (100% would correspond to the complete absence of saturation effects). The effective quantum yield ($\Phi_{\mathrm{eff}} = \Phi_0\Phi_{\mathrm{sat}}$) is thus estimated to be around 50%. We note that the precise numerical values of $\Phi_0\Phi_{\mathrm{sat}}$ and ΔV are uncritical for our conclusions on the sequence of proton and electron transfer events.

Deconvolution of raw PBD signals. Correction of the flash-induced PBD signals for (*i*) miss events resulting from the less-than-unity quantum efficiency in exciting S-state transitions by saturating flashes (8), (*ii*) blockage of higher S-state transitions in a PSII fraction devoid of the secondary acceptor quinone Q_B (non-Q_B units, ref. 9), and (*iii*) a small S_0-state population in the dark samples was done using the Kok model (8, 10). These corrections (also denoted as "deconvolution") yield the PBD signals attributable to the individual S-transitions between Kok's semistable S-states (Fig. 2). The applied correction procedure differed from the one detailed elsewhere (10) in two details only: (*i*) Double hits (centers hit twice by the same flash) were not included in the deconvolution model because of the use of nanosecond excitation laser flashes; and (*ii*) a possible small fraction of non-Q_B units in the S_2-state that recombines to the S_1-state in between two laser flashes was neglected.

The miss parameter, m, was determined from simulations of the pattern in a flash series of the approximately 1.6-ms rise in the PBD signals caused by transition $S_3 \rightarrow S_0$ (Fig. S1*B*), and took into account the temperature dependence of m as determined previously (11). At 20 °C, the best simulation was obtained using $m = 10\%$, 10% of non-Q_B centers, and a S_0-population of 5%, in agreement with previous determinations for the same PSII material and similar sample conditions (10, 12, 13).

The above-described deconvolution procedure only holds for those parts of the PBD signals that are caused by photochemical reactions of the photosystems. All kinetic phases visible in the PBD signals obviously have such an origin because the absorbed light energy that is not used photochemically is thermally deactivated rapidly (<1 μs). Excess energy thus contributes to the prompt PBD signal (offset). The effect of miss events on the prompt phase of the PBD signals is not quite clear; probably the whole energy contributes as heat to the prompt signal. The same holds for non-Q_B centers in the S_2-state. We thus confined ourselves to performing the deconvolution for the kinetic phases ($\tau > 10$ μs) of the PBD signals. Prompt phases were not deconvoluted.

We emphasize that no central conclusions of this work depend critically on the details of the correction (see Fig. S2 for comparison of uncorrected and corrected transients).

1. Berthold DA, et al. (1981) A highly resolved, oxygen-evolving photosystem II preparation from spinach thylakoid membranes: EPR and electron-transport properties *FEBS Lett* 134:231–234.
2. Schiller H, Dau H (2000) Preparation protocols for high-activity photosystem II membrane particles of green algae and higher plants, pH dependence of oxygen evolution and comparison of the S2-state multiline signal by X-band EPR spectroscopy. *J Photochem Photobiol B* 55:138–144.
3. Krivanek R, Dau H, Haumann M (2008) Enthalpy changes during photosynthetic water oxidation tracked by time-resolved calorimetry using a photothermal beam deflection technique. *Biophys J* 94:1890–1903.
4. Klauss A, Krivanek R, Dau H, Haumann M (2009) Energetics and kinetics of photosynthetic water oxidation studied by photothermal beam deflection (PBD) experiments. *Photosynth Res* 102:499–509.
5. Gensch T, Viappiani C (2003) Time-resolved photothermal methods: Accessing time-resolved thermodynamics of photoinduced processes in chemistry and biology. *Photochem Photobiol Sci* 2:699–721.
6. Braslavsky SE, Heibel GE (1992) Time-resolved photothermal and photoacoustic methods applied to photoinduced processes in solution. *Chem Rev* 92:1381–1410.
7. Schulenberg PJ, Gärtner W, Braslavsky SE (1995) Time-resolved volume changes during the bacteriorhodopsin photocycle: A photothermal beam deflection study. *J Phys Chem* 99:9617–9624.
8. Kok B, Forbush B, McGloin M (1970) Cooperation of charges in photosynthetic O_2 evolution, I. A linear four-step mechanism. *Photochem Photobiol* 11:457–475.
9. Lazar D (1999) Chlorophyll a fluorescence induction. *Biochim Biophys Acta* 1412:1–28.
10. Gerencsér L, Dau H (2010) Water oxidation by photosystem II: H_2O–D_2O exchange and the influence of pH support formation of an intermediate by removal of a proton before dioxygen creation. *Biochemistry* 49:10098–10106.
11. Grabolle M, Dau H (2007) Efficiency and role of loss processes in light-driven water oxidation by PSII. *Physiol Plant* 131:50–63.
12. Grabolle M, Dau H (2005) Energetics of primary and secondary electron transfer in photosystem II membrane particles of spinach revisited on basis of recombination-fluorescence measurements. *Biochim Biophys Acta* 1708:209–218.
13. Haumann M, et al. (2005) Photosynthetic O_2 formation tracked by time-resolved x-ray experiments. *Science* 310:1019–1021.

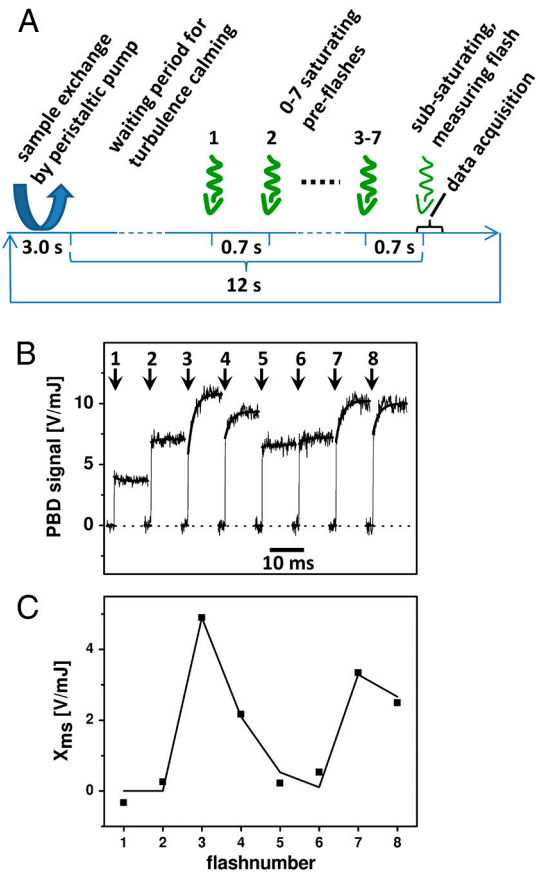

Fig. S1. (*A*) Experimental laser-flash protocol. Saturating laser flashes, spaced by 0.7 s, populate predominantly a specific semistable S-state in the initially dark-adapted PSII sample. The subsaturating measuring laser flash is applied 0.7 s after the last saturating flash. The PBD signal was recorded in an interval of 8 ms before and 16 ms after the measuring laser pulse. A peristaltic pump runs for 3 s to exchange the sample in the flow-through cuvette. During this 3-s pumping approximately 0.5 mL of the sample from the ice-cooled dark reservoir reach the heat exchanger, wherein the sample is thermostated in a thin-walled silicon tube during the remaining 12 s of the measuring cycle. Simultaneously, the compartment of the thermostated flow-through cuvette is filled with a thermostated sample from the heat exchanger. Before the next measurement cycle is started, it is necessary to wait several seconds until turbulences in the cuvette have calmed down. (*B*) PBD signals in a series of eight flashes (at 20 °C) showing quaternary oscillation of the millisecond rising phase caused by transition $S_3 \rightarrow S_0$. Spacing between two flashes was 700 ms. (*C*) Amplitude pattern (squares) of the ms phase (X_{ms}) and simulation (line) based on the Kok model, using a miss factor of 10%, 10% of non-Q_B centers, and a 5% population of the S_0-state in the dark.

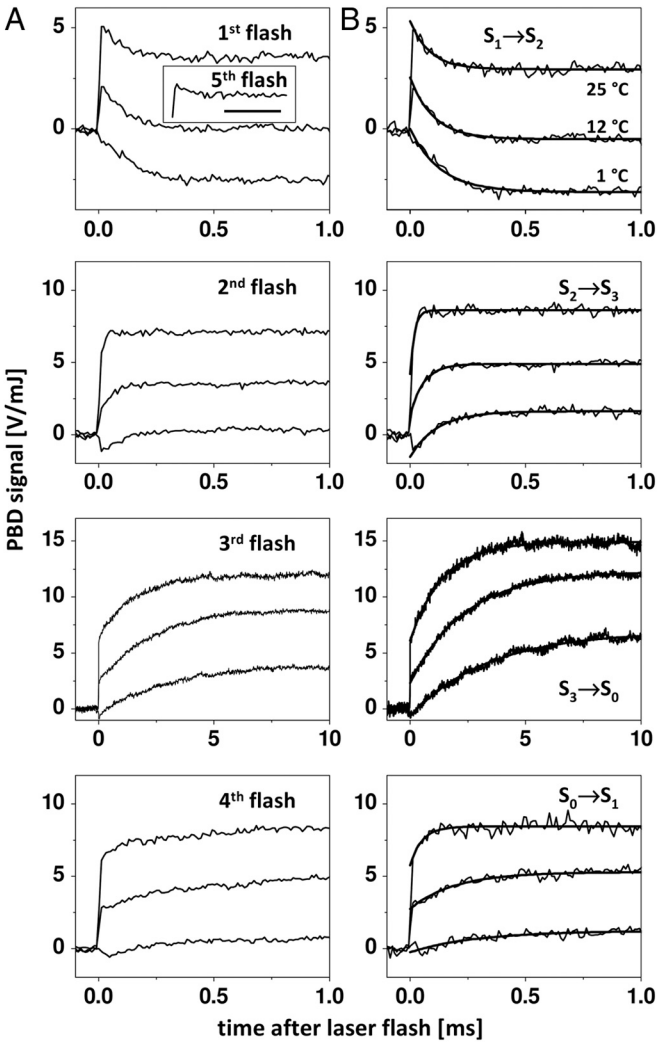

Fig. S2. (*A*) PBD signals induced by laser flashes 1, 2, 3, and 4 applied to dark-adapted PSII membrane particles at three measuring temperatures. For the signals, approximately 400 transients each from a fresh PSII sample were averaged. (*Inset*) The signal induced by flash 5 at 25 °C (the bar denotes 250 μs). A decay phase with a time constant of approximately 100 μs is visible on the signal induced by the first flash as well as the fifth flash. Thus, it can be excluded that this feature of the signal induced by the first flash is caused by inactive PSII centers on the first excitation only. (*B*) PBD signals of transitions $S_1 \rightarrow S_2$, $S_2 \rightarrow S_3$, $S_3 \rightarrow S_0$, and $S_0 \rightarrow S_1$ derived after deconvolution (correction for a miss factor of 11% at 1 °C, 9% at 12 °C, and 11% at 25 °C, 10% of non-Q_B centers, and a 5% population of the S_0-state in the dark) of the signals in *A*. Thin lines, experimental data; thick lines in *B*, simulations using a step-shaped function for the rapid jump caused by $Q_A^- Y_Z^+$ formation and single-exponential functions for the slower signal contributions.

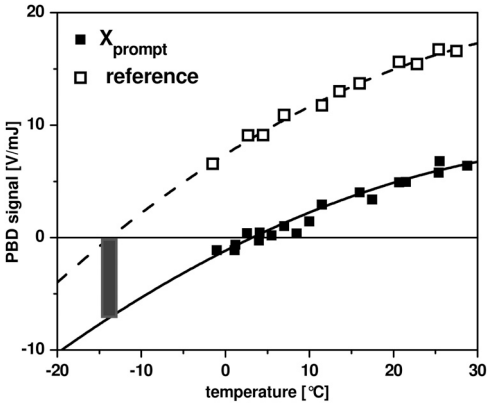

Fig. S3. Temperature dependence of the initial rapid PBD signal of PSII and of an intrinsic calorimetric reference. Filled squares indicate averaged amplitudes of PBD signals (X_{prompt}) from PSII on flashes 1–4 at approximately 5 μs after each flash (derived from simulations of flash transients; see Fig. S2). As intrinsic reference we used the standard PSII sample, added 50 μmol/L 3-(3,4-dichlorophenyl)-1,1-dimethylurea (DCMU), and applied saturating background light from a green LED. Under those conditions, Q_A^- remains permanently reduced. Light absorbed by those "closed" reaction centers cannot induce a long-living charge separation, and the absorbed light energy is mostly released as heat (ΔQ) within <1 μs. The requirements for a calorimetric reference are thus fulfilled as long as losses caused by fluorescence are neglected. Open symbols represent the scaled, prompt amplitude of the intrinsic reference. This dataset was used only to determine the ratio of the parameters α, β, and γ by simulation of the temperature dependence with a second-order polynomial [$X_Q(T) = \alpha + \beta T + \gamma T^2$]. For the temperature, T_0, at which the thermal part of the PBD signal vanishes (i.e., the signal of a reference vanishes), we obtained a value of −14 °C, in good agreement with earlier estimates (3). The prompt negative amplitude of PSII at T_0 (indicated by the grey bar) directly gives the nonthermal contribution to the PBD signal and can be interpreted as an apparent contraction caused by $Y_Z^+Q_A^-$ formation. In previous investigations in our laboratory we determined the heat release ΔQ upon formation of the charge pair $Y_Z^+Q_A^-$ to be 76.4% for an excitation energy of 5 μJ using a more sophisticated calorimetric standard consisting of a mixture of PSII and the dye BCP (3). Referring to those results and using the equation $X(T) = X_Q(T)\Delta Q + \Delta N$ with $\Delta N = 0$, we calculated the absolute values $\alpha = 7.3899$, $\beta = 0.4799\ °C^{-1}$, and $\gamma = -0.0048\ °C^{-2}$ by the assumption that $\Delta Q = 80\%$ for the simulation of the prompt PSII signal (solid line) and $\Delta Q = 100\%$ in the case of the intrinsic reference (dashed line). The same values of α, β, and γ, and the above equation were used to simulate the temperature dependence of PBD signals caused by the S-transitions to determine respective values of ΔQ and ΔN. From ΔN, apparent volume changes ΔV were calculated using Eq. **S1**.

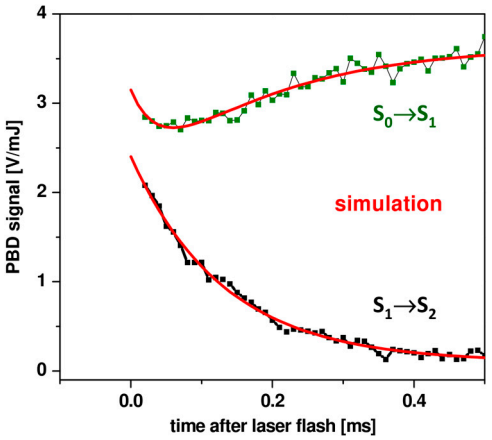

Fig. S4. Rapid decay phase in the $S_0 \rightarrow S_1$ transition (in D_2O at 20 °C). PBD signals of the $S_1 \rightarrow S_2$ transition (black) and $S_0 \rightarrow S_1$ transition (green) for PSII membranes in D_2O are shown. Red lines represent simulations with a single-exponential function plus offset for the $S_1 \rightarrow S_2$ transition ($A = -2.30$ V/mJ, $\tau = 131$ μs) and the sum of two exponential functions ($\tau_1 = 40$ μs, $\tau_2 = 186$ μs, $A_1 = -1.12$ V/mJ, $A_2 = 1.61$ V/mJ) plus offset for the $S_0 \rightarrow S_1$ transition. The experimental signal of the $S_0 \rightarrow S_1$ transition in D_2O shows a rapid initial decay phase that is well-simulated with a time constant of 40 μs (red line). At low temperatures in H_2O there are also indications for a rapid decay phase in the PBD signal of the $S_0 \rightarrow S_1$ transition (see Fig. S2). This contribution is small, close to the noise level, and thus uncertain. Because of its similar τ-value, it may be assignable to the electron transfer (ET) from the Mn complex to Y_Z^{ox} in the $S_0^n \rightarrow S_1^+$ transition, and is possibly associated with a volume contraction, which is clearly smaller than the one observed for the ET in the $S_1^n \rightarrow S_2^+$ transition. In H_2O at room temperature such a rapid decay phase was not discernable, probably because it is kinetically not well-separated from the dominant rising phase of the PBD signal. We consider these results as further evidence that the proton transfer in the $S_1^+ \rightarrow S_1^n$ transition ($\tau_2 = 186$ μs) occurs only after the ET ($\tau_1 = 40$ μs) from the Mn complex to Y_Z^{ox} in the $S_0^n \rightarrow S_1^+$ transition (Fig. 1*B*).

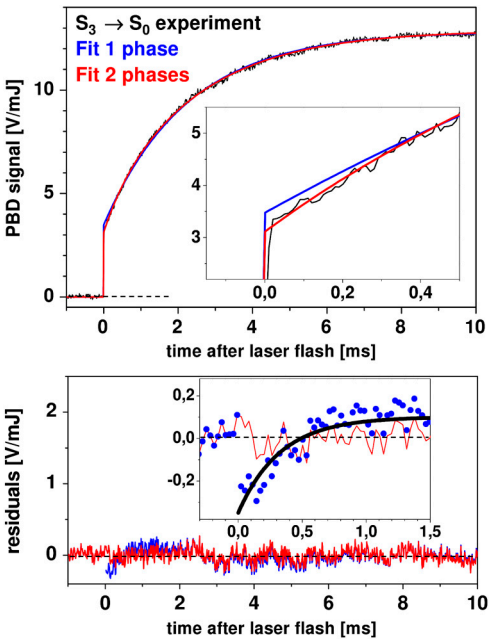

Fig. S5. PBD transient of the $S_3^+ \rightarrow S_0^n$ transition and simulations. (*Top*) PBD signal at a mean temperature of approximately 14 °C, representing the average of signals in a temperature range of 1–25 °C, for improvement of the signal-to-noise ratio, and both monoexponential (blue) and double-exponential (red) simulations. (*Top, Inset*) The first half-millisecond on an expanded time scale, revealing a clear deviation of the monoexponential fit from the experimental data, but a better fit for the biexponential simulation ($\tau_1 = 430$ μs, $\tau_2 = 2.3$ ms, $A_1 = 0.95$ V/mJ, $A_2 = 8.87$ V/mJ). (*Bottom*) Residual plots of data in the top figure. (*Bottom, Inset*) The experimental data on an expanded time scale (at a resolution of 30 μs per data point) and, in addition, a fit of the residuals from the monoexponential simulation with an exponential rise (black) with a τ-value of 360 μs and an amplitude of 0.45 V/mJ. Previous experiments have revealed a phase in the hundreds of microseconds time range, which precedes the O_2 release-associated millisecond phase and manifests as a lag phase in time-resolved X-ray absorption spectroscopy (XAS) and UV signals (10, 13). Such a lag phase is not observed in the PBD signal. Instead, comparison of mono- and double-exponential simulations of the signal reveals a residual rising phase for the monoexponential fit, which disappears if a second phase with a τ-value of 320 μs is included in the simulation. We attribute this volume change to a proton transfer reaction in the $S_3^+ \rightarrow S_3^n$ transition before ET and concomitant O_2 release in the $S_3^n \rightarrow S_0^n$ transition (10, 13). In the $S_3 \rightarrow S_0$ transition (flash 3), Y_Z^+ formation is therefore followed by three processes that we predict to be associated with a volume expansion: (*i*) One proton is removed from the Mn complex within about 200 μs (at room temperature, $S_3^+ \rightarrow S_3^n$ in Fig. 1*B*); in analogy to the proton removal step in the $S_2^+ \rightarrow S_2^n$, this discharging of the donor side could result in a volume expansion (approximately 4 Å^3). (*ii*) The rate-limiting ET from the Mn complex to Y_Z^+ ($S_3^n \rightarrow S_4^+$, τ around 2 ms) is coupled to Mn reduction in the O—O bond formation step and thus to the reversal of the contraction associated with Mn oxidation in the $S_1^n \rightarrow S_2^+$ transition (approximately 6 Å^3). (*iii*) A second proton is released immediately before or after O—O bond formation ($S_0^+ \rightarrow S_0^n$ in Fig. 1*B*), likely also associated with a volume expansion (approximately 4 Å^3). In our PBD experiment, the above three steps are not well-resolved as separate processes so that, to a first approximation, the experimentally determined expansion by about 4 Å^3(*i*) + 6 Å^3(*ii*) + 4 Å^3(*iii*) = 14 Å represents the sum of the individual contributions. The numerical agreement between predicted (14 Å^3) and experimentally determined (15 Å^3) volume changes is reassuringly good but also might be fortuitous. Thus, it remains an open question whether, in addition to the discussed three contributions, O—O bond formation and O_2 release itself also contribute to the experimentally observed volume change during the $S_3 \rightarrow S_0$ transition.

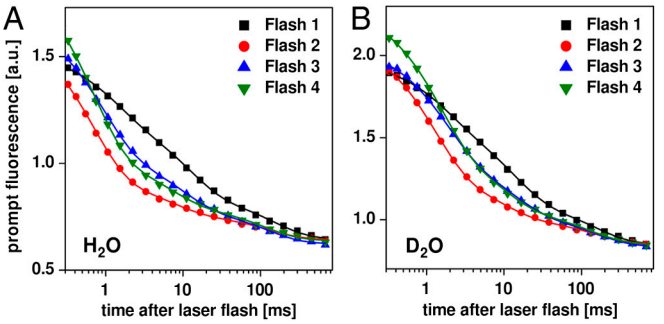

Fig. S6. Decay of the chlorophyll fluorescence yield (prompt chlorophyll fluorescence) after Q_A^- formation by laser-flash excitation for PSII in H_2O (*A*) and D_2O (*B*). A sequence of saturating laser flashes (flash 1, flash 2, etc.) to dark-adapted PSII membrane particles and the variability in the fluorescence yield (1) was detected by LED probe pulses using a commercial instrument (FL3000; Photo Systems Instruments). Symbols show the experimental data; lines represent the results of multiexponential simulations. This experiment was employed to monitor the oxidation of Q_A^- formed after excitation by a saturating laser flash. The fluorescence yield is maximal for reduction of Q_A in all PSII (F_m) and minimal for oxidized Q_A (F_0) (1); the multiphasic decay reflects the quinone redox chemistry. [Additional factors influence the yield of the prompt chlorophyll fluorescence; the flash-number dependence of the initial level of $F(t)$ does not indicate a variation in the amount of reduced Q_A but a minor influence of the PSII donor side on the fluorescence yield.] The fluorescence decay was well-described by the sum of three exponential functions plus offset. Values for the smallest of the three time constants (fastest decay phase), τ_1, and the corresponding relative amplitudes, A_1, are given in Table S1. This phase is attributed to electron transfer from Q_A^- to a secondary quinone molecule (Q_B or DCBQ) at the PSII acceptor side (2, 3). Except for the $S_3^n \rightarrow S_0^n$ transition, the fastest acceptor-side ET step was considerable slower than any of the PBD signals associated with the S-state transitions (compare Table 1) and also slower than the ET from the Mn complex to Y_Z^+ (see Table 2), both in D_2O and in H_2O. The influence of PBD signals caused by the relatively slow acceptor-side reactions on the determination of the time constant for the most rapid PBD phases attributed to the donor side was studied for the $S_0 \rightarrow S_1$ and $S_2 \rightarrow S_3$ transitions, as shown in Fig. S7.

1 Dau H (1994) Molecular mechanisms and quantitative models of variable photosystem II fluorescence. *Photochem Photobiol* 60:1–23.
2 de Wijn R, van Gorkom HJ (2001) Kinetics of electron transfer from Q_a to Q_b in photosystem II. *Biochemistry* 40:11912–11922.
3 Krivanek R, Kern J, Zouni A, Dau H, Haumann M (2007) Spare quinones in the Q_B cavity of crystallized photosystem II from *Thermosynechococcus elongatus*. *Biochim Biophys Acta* 1767:520–527.

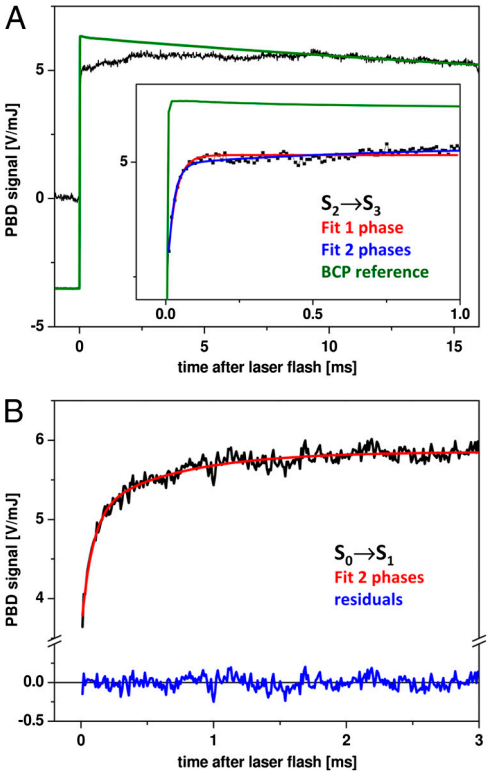

Fig. S7. PBD signal of the $S_2 \rightarrow S_3$ (*A*) and $S_0 \rightarrow S_1$ transition (*B*). In *A*, the PBD signal of the $S_2 \rightarrow S_3$ transition detected at 20 °C in H_2O is shown for about 15 ms after laser-flash excitation (black); (*Inset*) the same signals on an expanded time scale. The signal (green) of the calorimetric reference dye, BCP, detected at the same temperature, shows a slow decay that can be attributed to heat diffusion because the BCP signal is of purely thermal origin. (For better comparison to the slow decay of the PSII signal, the BCP signal was scaled and offset.) The difference between the black and green transients in the first few milliseconds after flash excitation points toward a small volume expansion possibly associated with acceptor-side processes. As compared to a monophasic simulation (red curve) and for times exceeding 15 μs, the PBD signal on the $S_2 \rightarrow S_3$ transition was indeed better simulated including both the rapid rising phase discussed in the main text and an additional small rising phase with the same τ-value (of 660 μs) obtained from the prompt fluorescence measurements (Fig. S6) and attributed to the ET at the acceptor side of PSII (blue curve). Respective fit results are listed in Table S2. The time constant determined for the rapid rise on the $S_2 \rightarrow S_3$ transition, however, was only marginally affected by the use of either monophasic or biphasic simulations of the PBD signal, both in H_2O and D_2O; also, the kinetic isotope effect (KIE) value was not affected significantly (Table S2). According to these results, the ET at the acceptor side seems to contribute small rising components to the PBD signals, so that the net volume changes caused by contractions and expansions at the donor side ($Y_Z^{ox}Q_A^-$ formation, Mn oxidation, proton transfer) and at the acceptor side (interquinone ET and proton transfer) of PSII may be close to zero when summed over the four transitions between semistable S-states of one turnover of the S-state cycle. (*B*) The PBD signal of the $S_0 \rightarrow S_1$ transition is shown (for PSII membranes at 20 °C in H_2O). The red line represents a simulation with the sum of two exponential functions plus offset for a fit range of 3 ms. Beside the rapidly rising phase, a slower rising phase with the same τ-value as determined from the prompt fluorescence decay for the acceptor-side ET was included (Table S1). The slower phase presumably reflects a volume expansion associated with interquinone electron transfer. Fit parameters for mono- or biphasic simulations of the PBD signals on the $S_0 \rightarrow S_1$ transition are summarized in Table S2. Variations of the time range of data used for the fits reveal that monophasic simulations are insufficient, because they result in an increase of the time constant for the rapid rising phase and in a decrease of the KIE with increasing fit range. The biphasic simulation yields a superior fit quality (low residuals level, blue line) and reveals a KIE of the rapid rising phase of 3.0 (Table S2), which we consider to be the most likely KIE value for the $S_0^+ \rightarrow S_1^n$ transition (Table 2).

Table S1. Fit parameter of triexponential simulations of the fluorescence decays of Fig. S6

	In H_2O		In D_2O	
	τ_1 (μs)	A_1 (%)	τ_1 (μs)	A_1 (%)
1st Flash	1,260	34	1,600	31
2nd Flash	660	71	1,260	66
3rd Flash	880	59	1,760	55
4th Flash	660	69	1,450	60

The smallest time constant (τ_1) obtained by a fit with a sum of three exponential functions (plus an offset) of the fluorescence signals on flash 1, 2, 3, and 4 (Fig. S6) are listed for measurements in H_2O and in D_2O (PSII membrane particles at 20 °C). Respective signal amplitudes (A_1) are given in % of the total signal magnitude (sum of A_1, A_2, and A_3).

Table S2. Time constants (τ_i), amplitudes (A_i), KIE, and error measure ($1 - R^2$) as derived from monophasic* or biphasic† simulations of PBD transients of the $S_2 \rightarrow S_3$ and $S_0 \rightarrow S_1$ transitions (Fig. 4 and Fig. S7)

Fit range	Parameter	H_2O	D_2O	KIE	$(1 - R^2)^‡$ (‰)
$S_2 \rightarrow S_3$ Monophasic simulation					
1 ms	τ_1 (μs)	29	162	5.6	9.8
	A_1 (V/mJ)	2.88	2.37		
$S_2 \rightarrow S_3$ Biphasic simulation					
1 ms	τ_1 (μs)	22	124	5.6	6.7
	A_1 (V/mJ)	3.03	2.12		
	τ_2 (μs)	660§	1,260§		
	A_2 (V/mJ)	0.38	0.76		
$S_0 \rightarrow S_1$ Monophasic simulation					
0.5 ms	τ_1 (μs)	118	603	5.2	7.2
	A_1 (V/mJ)	1.77	1.75		
3 ms	τ_1 (μs)	271	585	2.2	12.2
	A_1 (V/mJ)	1.67	1.45		
$S_0 \rightarrow S_1$ Biphasic simulation					
3 ms	τ_1 (μs)	84	261	3.0	9.5
	A_1 (V/mJ)	1.45	0.93		
	τ_1 (μs)	660§	1450§		
	A_1 (V/mJ)	0.79	0.82		

*Monophasic simulation: single-exponential function plus offset.

†Biphasic simulation: sum of two single-exponential functions plus offset.

‡As a measure of the goodness of the fit, the adjusted R^2 value was calculated using Origin (OriginLab, version 8.5). Herein, we present the value of $1 - R^2$. A lower value of $1 - R^2$ (closer to zero) indicates a better fit. We note that the R^2 value represents the goodness of the fit, also taking into account the number of fit parameters. This means that for a fit range of 3 ms, the biphasic simulation of the $S_0 \rightarrow S_1$ transient is indeed superior to the monophasic simulation.

§Indicates that the respective time-constant values were taken from the results of the prompt-fluorescence analysis (Table S1) and kept constant (fixed) in the simulations. The corresponding experimental data and simulations are shown in Fig. S7 (and also, for the $S_0 \rightarrow S_1$ transition, in Fig. 4*D*).